ISSN 2228-9860 eISSN 1906-9642 CODEN: ITJEA8

International Transaction Journal of Engineering, Management, & Applied Sciences & Technologies

http://TuEngr.com

# Integration of Virtual Resistor in Charging Control System of Electric Vehicles to Mitigate the Harmonic Issues at Power Grid Side

**Ali S. Alghamdi**[1*]

[1] *Department of Electrical Engineering, College of Engineering, Majmaah University, Majmaah 11952, SAUDI ARABIA.*

**Corresponding Author (Email: aalghamdi@mu.edu.sa)*

**Paper ID: 12A3T**

**Volume 12 Issue 3**

Received 04 November 2020
Received in revised form 23 December 2020
Accepted 20 January 2021
Available online 26 January 2021

**Keywords:**
Bi-directional converter; Electric vehicle (EV); Inverter, EV Battery; Distortion control; Filter; PHEV; AC-DC Converter Control; Virtual resistance; Virtual resistor; Total harmonic distortion (THD); Smart Grid; Electric power quality.

## Abstract

The frequency of using electric vehicles (EVs) is nowadays on the rise as these vehicles are efficient and popular among people. However, the charging problem is the principal issue in EVs. This article tries to advance the harmonics of EVs charging via a virtual resistor and to assess its efficacy in promoting the battery health of EVs through its comparison with the absence of a virtual resistor. According to the simulation findings, the input current continues entirely in the introduced two-way converter; consequently, a significant reduction occurs in the input current total harmonic distortion (THD) in comparison to a conventional converter. Also, a THD of 4.5% observed for the output current by the introduced converter demonstrating its effectiveness, while satisfying the standard THD value lower than 5%. Besides the reduced THD rate, the THD of current turns to 3.67% following the application of the virtual resistor, which corresponds to the standard. Moreover, this value is 0.86% lower than the harmonic value of the system in the first case (with no use of virtual resistance), suggesting that the introduced approach is effective.

**Disciplinary**: Electrical Power Systems Engineering, Control Systems Engineering, Electrical System Operation.



## Cite This Article:

Alghamdi, A. S. (2021). Integration of Virtual Resistor in Charging Control System of Electric Vehicles to Mitigate the Harmonic Issues at Power Grid Side. *International Transaction Journal of Engineering, Management, & Applied Sciences & Technologies, 12*(3), 12A3T, 1-16. http://TUENGR.COM/V12/12A3T.pdf DOI: 10.14456/ITJEMAST.2021.62

## 1 Introduction

Recently, a variety of environmental-friendly vehicles, including all-electric vehicles (EVs) and plug-in hybrid electric vehicles (PHEVs), being highly promising to decrease pollutants in the environment, have gained ground among the public [1]-[3]. The propulsion batteries supply all the

power needed by EVs; these batteries are recharged using an on-board charger be connecting to the power grid. Thus, these chargers play a vital role in the operation of electric vehicles [4].

The charger's performance can be assessed by examining the efficiency of power conversion and the electric power quality based on criteria such as THD and power factor). Moreover, the charger should enjoy necessary features such as small size, low weight, and prolonged lifespan to be installed in the EVs. The routine on-board chargers are used in electric vehicles (EVs), based on the two-stage structure isolated AC-DC converters, including the power-factor-correction (PFC) and the DC-DC power-conversion stages [5]-[7].

Currently, there are ongoing investigations on two major EV charging solutions, i.e. induction and conduction approaches. The major difference between conduction and induction is that conduction allows the charging of EVs with the electrical power grid by forming direct contact with it. While induction is the process of charging EVs by the electrical power grid without making any direct contact [8]. In spite of recently reported developments in the inductive technique [9], [10], the conductivity approach has been the basis of widely used solutions [11]. The designing process in the majority of EVs is based on the conduction technique of one-way battery chargers characterized by IEC 61851-1, modes 1 to 3 [12]. The operation of such one-way battery chargers is merely possible in the conventional G2V mode to charge the traction batteries by the electrical grid. Besides inside-embedded battery chargers, the batteries in some vehicles can be charged by one-way off-board chargers with the specifications of IEC 61851-1, standard 4 modes.

A multipurpose topology presented in [13] enables the energy to be exchanged between two batteries with dissimilar voltages. Such a topology is used for charging auxiliary batteries with traction batteries. Based on IEC 61851-1, however, traction batteries must be separated from the car chassis. Thus, this requires separated DC-DC topologies. An attractive isolated topology presented in [14] provides the ability to recharge the auxiliary battery with the energy that comes from traction batteries; even so, a multitude of power-controlled semiconductors are required in this topology. Optimal management of EVs in charging stations for participating in regulation and energy market using advanced reservation model was presented in [15]. A bi-level programming model was proposed in [16] for minimizing social cost to optimally determine the charging service fee of charge stations considering operational constraints of EVs and electrical distribution systems. To cover the uncertainties of future EV charging demand, an optimization model with the aim of reducing the peak of electricity demand at an EV parking lot in the presence of photovoltaic arrays by taking into account the uncertainties related to the arrival time of EV as well as the amount of energy demand was proposed in [17]. An approach to establishing practical planning of EVs in parking lots considering slow-charging EVs as a regulation service and mitigating high fluctuation of fast-charging EVs using slack power resources was introduced in [18]. In [19] a new structure using mathematical model extraction to charge the dynamics of electric vehicles was proposed and its practical results were presented to validate the model.

To the best of the author's knowledge, very few works have considered the effects of harmonic problems associated with the EVs charging systems on the electric grids and how to mitigate them. In the present article, a simple, inexpensive, and effective solution is presented that utilizes a battery charger topology on a reconfigurable board, which also enables operating in Grid-to-Vehicle (G2V) as well as Vehicle-to-Grid (V2G) states. The auxiliary traction is performed with no extra converters as battery charging operation functions properly.

# 2 Battery charger control

## 2.1 Overview of a reconfigurable battery charger system

The electrical schematic of the reconfigurable onboard battery charger system (without a virtual resistor) including three main power stages is shown in Figure 1.

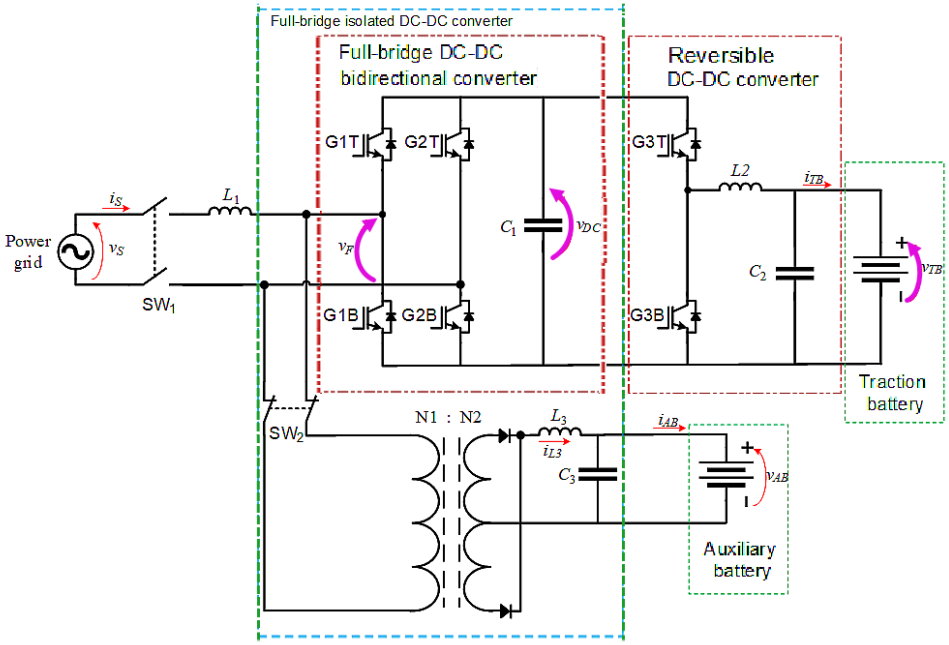


**Figure 1**: Reconfigurable battery charger system [20]

The current in the individual converters is dependent upon the operational modes. Figure 2 depicts the power supply of an adjustable battery charger in a range of operational modes. The G2V and V2G operational modes are shown in Figure 2 (a). In the G2V mode, the active power, *P*, flowing from the electrical network, energized the DC link and then flows into the traction batteries, while it flows inversely in the V2G mode. The reactive power, *Q*, can be adjusted by the battery charger in these two modes, if needed. Figure 2 (b) displays the operation of T2A, where the flow of energy is from traction batteries to auxiliary batteries.

The following description analyzes the performance of an adjustable battery charger for each performance mode.

## 2.2 Virtual Resistance Concept

To reduce the great fluctuation of the passage in the LC circuit, the resistor can be integrated with the LC circuit, which is a concept understandable by the whole electric engineers. Despite the

high effectiveness of temporary oscillation damping by resistors, the technique is not practical because of excess loss rates in the resistor.

The basics of the introduced virtual resistance concept are to understand the very fundamental damping notion of a transitory fluctuation in a resonant circuit (LC circuit) with the help of a resistor. The one-way AC equivalent side circuit of a three-phase AC/DC PWM converter is shown in Figure 3 (a). In the AC-DC PWM converter, the key element of the input current phase seems to be the current source $I_{in}$. The circuit dynamic behavior as shown in Figure 2 (a) can be analyzed according to the block diagram depicted in Figure 3 (b) to achieve the transfer functions as follows:

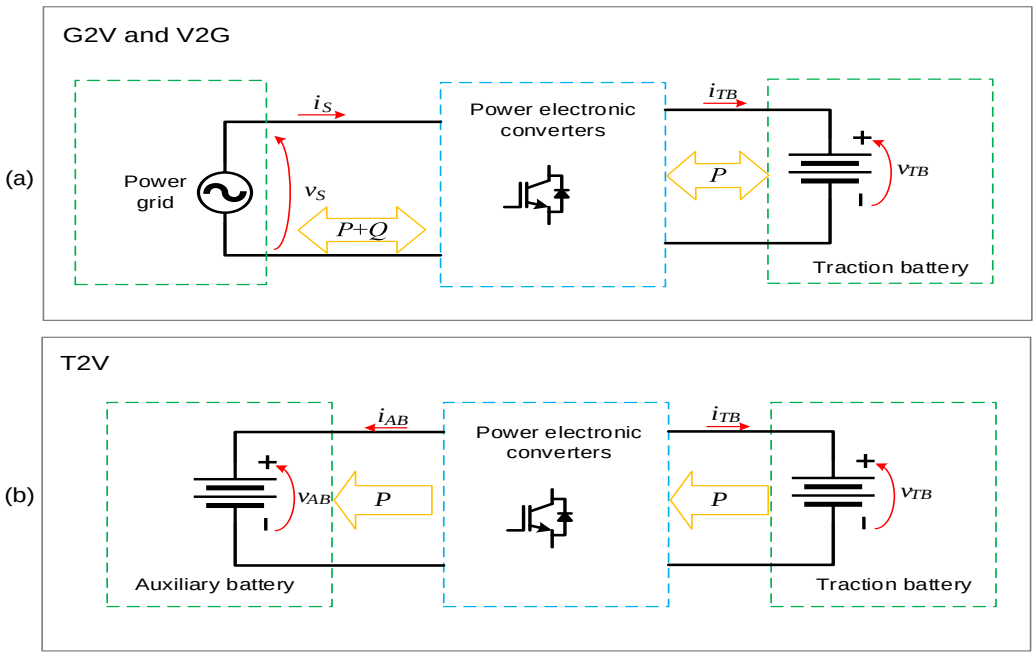


**Figure 2**: The power supply of a rechargeable battery charger: In G2V as well as V2G (a), and in the T2A (b) operational modes [20]

$$\frac{I_s(s)}{I_{in}(s)} = \frac{1}{1+s^2 L_f C_f} \tag{1}$$

$$\frac{V_{Cf}(s)}{I_{in}(s)} = -\frac{sL_f}{1+s^2 L_f C_f} \tag{2}$$

where

$I_s(s)$: The Laplace transformed of source current

$v_{Cf}(s)$: The filter capacitor voltage

$I_{in}(s)$: The converter input current

$s$: The Laplace operator.

According to (1) and (2), a sudden change in the converter's input current generates causes unexpected transients on the capacitor voltage and current source. Practically, this typically undergoes transient weakening with a minor loss in the LC circuit.

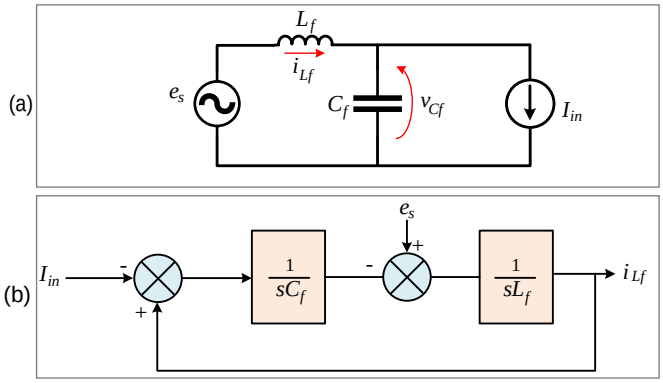


**Figure 3**: Equivalent AC-DC PWM circuit model at the AC side with block diagram

According to the block diagram represented in Figure 2(a), a resistor connected to the filter inductor serially is tasked to reduce the inductor incoming input voltage proportionate to its ongoing current. The manipulation of the block diagram in Figure 2(a) results in that in Figure 3(a). Figure 3(a) represents the system's behavior, which is similar to Figure 2(a) as the block diagram in Figure 3(a) exactly results from manipulating the block diagram in Figure 2(a). Rather than the use of an actual resistor, however, the current via the inductor is measured by the system in Figure 3(a) to represent the function of a resistor $R_I$ in series, which result is subjected to differentiation caused by a constant of $sCR_I$ (Figure 5). Thereafter, the differentiator output is introduced to the reference signal of the converter current. Therefore, the function of the real resistor connected serially to the filter inductor can be replaced using an extra differentiator as that presented in Figure 3(a). Nevertheless, the differentiator will not produce excess loss (which is desirable) but merely generates the resistor's damping impact. Accordingly, the differentiator, as observed in Figure 3(a), can be considered a virtual resistor serially connected to the filter inductor. A virtual resistor added to the filter (capacitor or inductor) serially or in parallel also be designed with a similar method. According to Figure 3, an extra current sensor and differentiator are required for connecting a virtual resistor serially to the filter inductor or the capacitor. Differentiators may cause noise problems due to amplifying high-frequency signals. To establish a virtual resistor connected in parallel to the filter inductor or the capacitor, a voltage sensor and an amplifier are needed. Thus, the implementation of such a virtual resistor will be so easier due to no need for a differentiator.

In practice, it is possible to use more than one virtual resistor concurrently. In the case of using two virtual resistors connected to the self-filter in parallel and serially to the capacitor, the reference input current ($i_{in}^{r^*}$) of the converter is computed as follows:

$$i_{in}^{r^*} = i_{in}^{r} + v_{Lf}/R_2 + sC_f R_3 i_{Cf} \quad (3),$$

Where, $i_{in}^{r} = [i_{in,u}^{r} \quad i_{in,v}^{r} \quad i_{in,w}^{r}]$ is the reference input current of converter obtained by the output voltage or the current controller, $v_{Lf} = [v_{Lf,u} \quad v_{Lf,v} \quad v_{Lf,w}]$ is the indicator's voltage of the filter, and $i_{Cf} = [i_{Cf,u} \quad i_{Cf,v} \quad i_{Cf,w}]$ is the capacitor's current of the filter.

Figure 4 depicts using a virtual resistor connected to an inductor filter in parallel and to the filter capacitor serially. It is possible to measure the voltage inside the inductor; to do so, the capacitor voltage is subtracted from the source voltage. Also, the capacitor's current in the filter is measured by subtracting the converter's input current absorbing from the source. From Equation (3), the modifier formulation of the converter's input current is similar to the form that was introduced in [1], which is according to the concept of state feedback:

$$i_{in}^{r^*} = i_{in}^{r} + k_1(e_s - v_{cf}) + k_2(i_s - i_{in}^{r}) \quad (4).$$

Where $e_s - v_{Cf} = v_{Lf}$ is the indicator's voltage of the filter, $i_s - i_{in}^{r} = iC_f$ is the capacitor's current of the filter. $k_1$ and $k_2$ are the real gain coefficients.

Considering $k_1$ equal to$1/R_1$, by substituting Equation (3) in Equation (4) would be on the last part of the equations. Based on a conclusion in [21], this mainly results from the fairly unimportant impact of $k_2$. Concerning the introduced concept as an opinion denoted by (3), we can consider the impacts of the two virtual resistors equivalent. Figure 4 displays a circuit with real resistors and virtual resistors.

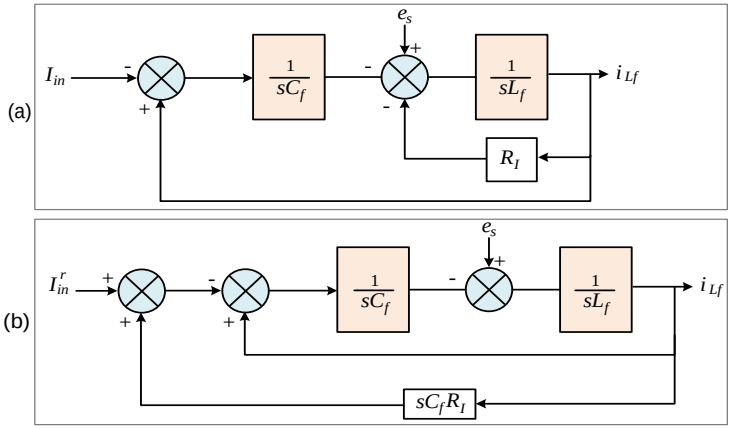


**Figure 4**: Schematic of the circuit with a real resistor (a) and a virtual resistor (b)

A comparison of Figure 3 and Figure 4 demonstrates that the virtual resistor presents its feedback and derivative in the control circuit. Figure 5 illustrates the PWM control circuit with a virtual resistor $R_3$.

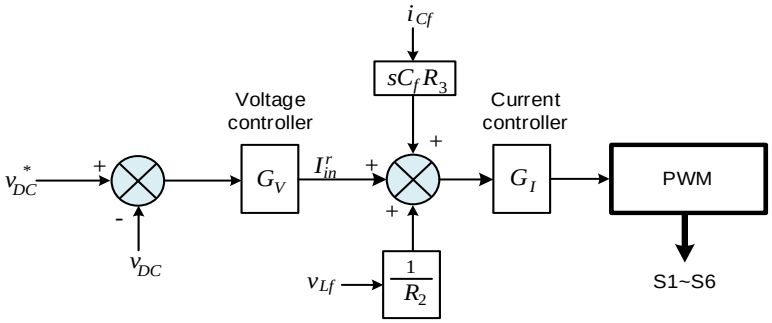


**Figure 5**: PWM Control circuit in the presence of a virtual resistor.

In the form of virtual resistors, they are characterized as coefficients in derivative feedback. All inputs and feedback are consolidated at the point to generate the PWM output. As denoted above, the existence of feedback and derivatives is the influence of virtual resistance.

This circuit is somehow derived from the formulas

$$i_{in}^{r*} = i_{in}^{r} + k_1(e_s - v_c) + k_2(i_s - i_{in}^{r}) \quad (5)$$

$$e_s - v_{Cf} = v_{Lf} \quad (6)$$

$$i_s - i_{in}^{r} = i_{Cf} \quad (7)$$

Equations (5)-(7) and the concept of aforementioned virtual resistance should be used to design the virtual resistance in the studied control circuit. For this purpose, we first generate two inputs of $v_{Lf}$ and $i_{Cf}$. These two parameters can be realized based on Figure 6.

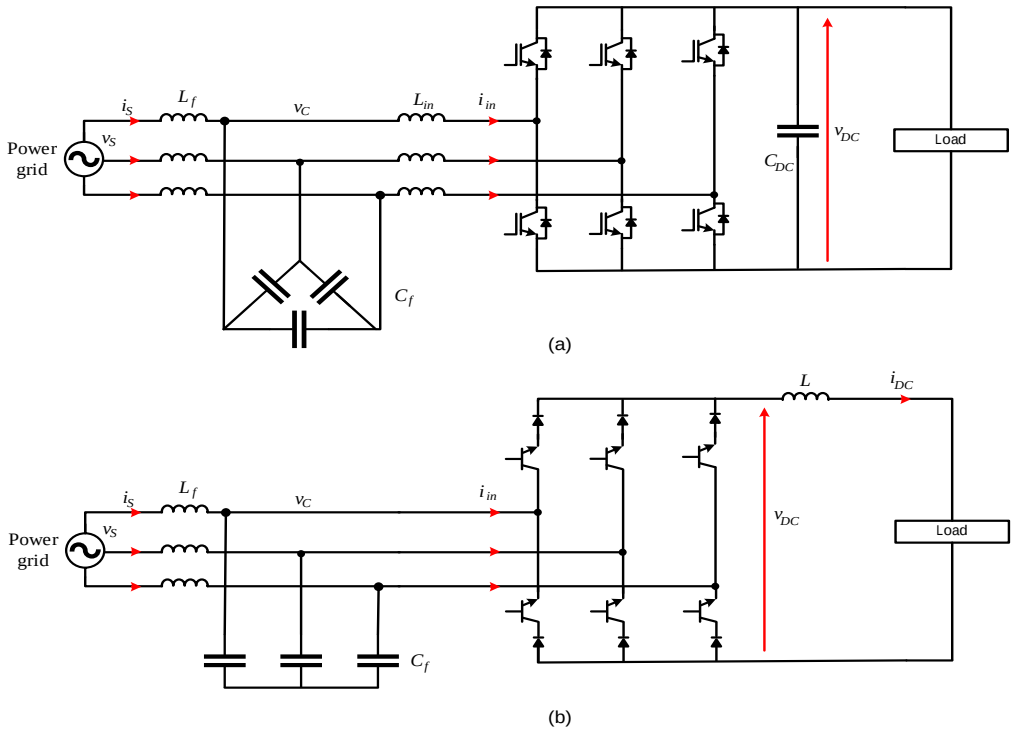


**Figure 6**: The AC/DC PWM converters Schemas. (a) Voltage-type and (b) Current-type.

Next, the inputs are connected to the PWM input by the creation of coefficients in their route. The feedback obtained from the voltage control block is also used to pack input Vdc. The control circuit will result in the existence of a virtual resistor. It is noteworthy that no change has occurred in the structure of the power circuit.

# 3 Control of charging and discharging modes

## 3.1 The Grid-to-Vehicle (G2V) Mode

$SW_1$ and $SW_2$ will be closed and opened, respectively, upon the operation of this mode (Figure 1). In this mode of operation, the DC-DC converter acts as a buck-type converter and the active AC-DC bidirectional rectifier is used to mitigate drowned current THD and control the power factor.

### 3.1.1 The Full-Bridge Bidirectional AC-DC Converter Control

The full-bridge bidirectional AC-DC converter controller must be synchronized with the fundamental voltage of the power grid to satisfy the allowable THD limit of the input current as defined in the IEC 61000-3-2 standard. Thus, the digital controller firstly implements a single-phase inverse Park Phase-Locked Loop (PLL) method. This algorithm transforms a voltage signal into two orthogonal components, commonly known as alpha-beta (α-β) transformation on a stationary reference frame. As seen from Figure 7, the components $pll_\alpha$ and $pll_\beta$ of input voltage signal are respectively made up by the PLL algorithm. Subsequently, these signals will be utilized as the input signals in the digital control circuit of the AC-DC rectifier for generating the current reference ($i_S^*$).

### 3.1.2 The Reversible DC-DC Converter Control

As the voltage magnitude of the traction battery is always lower than the voltage at the DC link, the reversible DC-DC converter functions as a buck converter throughout the G2V operation mode.

The constant-current and constant-voltage are two general charging stages recommended by most producers of EV batteries. First, with constant-current, the battery is charged until reaching the suggested maximum voltage. Then, the battery will be charged with constant-voltage until it reaches the predefined residual current limit. In the constant-current stage, as shown in Figure 8, a comparison is made between actual and the reference currents; a PI controller is then fed by the resulting error to adjust the output duty-cycle by a PWM modulator equipped with a 40 kHz triangular carrier. The control algorithm will change into the constant-voltage stage, as the traction battery's voltage gets to the maximal value suggested by the manufacture. The voltage is kept constant by using another PI controller.

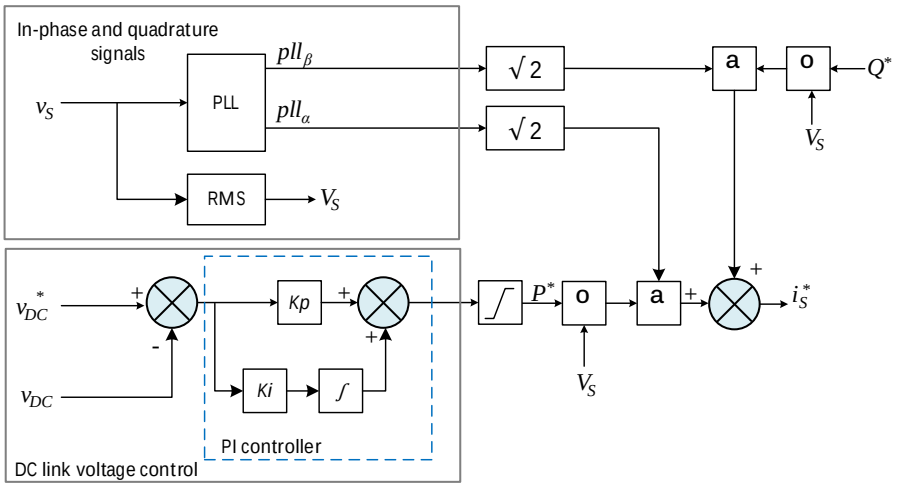


**Figure 7**: The control block diagram of the full-bridge bidirectional AC-DC converter

## 3.2 The Vehicle-to-Grid (V2G) Mode

The $SW_1$ and $SW_2$ are respectively closed and opened throughout this operation mode (see Figure 1). In this mode of operation, the DC-DC converter acts as a boost-type converter and the active AC-DC bidirectional converter acts as an inverter ensuring purely sinusoidal current delivery to the power network.

### 3.2.1 The Full-Bridge Bidirectional AC-DC Converter Control

It is necessary to synchronize the full-bridge bidirectional AC-DC converter with the fundamental voltage of the power grid to operate properly. A single-phase α-β PLL is used for the synchronization process. By defining *pll*α and *pll*β as the synchronization signals, they will be utilized as inputs for the succeeding digital control algorithms. A combination of active and reactive power can be utilized to generate current reference *is**. Future Smart Grid integration is enabled by establishing these powers while external input parameters are obtained from a digital port. Having all these in mind, the control algorithm applied in the V2G mode resembles that utilized in the G2V mode.

A predictive method can be implemented to estimate the reference current. The reference voltage estimated also by the predictive method combining with a 20 kHz triangular carrier is used to generate gate pulse sample using a unipolar sinusoidal PWM. Besides, this operational mode uses dead-time compensation procedure.

### 3.2.2 Reversible DC-DC Converter Control

A DC link voltage larger than the power grid peak value is needed to deliver back the energy stored in the traction batteries using the full-bridge AC-DC bidirectional converter to the power grid. The reversible DC-DC converter should function as a step-up converter (boost converter) due to the lower voltage of the traction batteries than the needed DC link voltage.

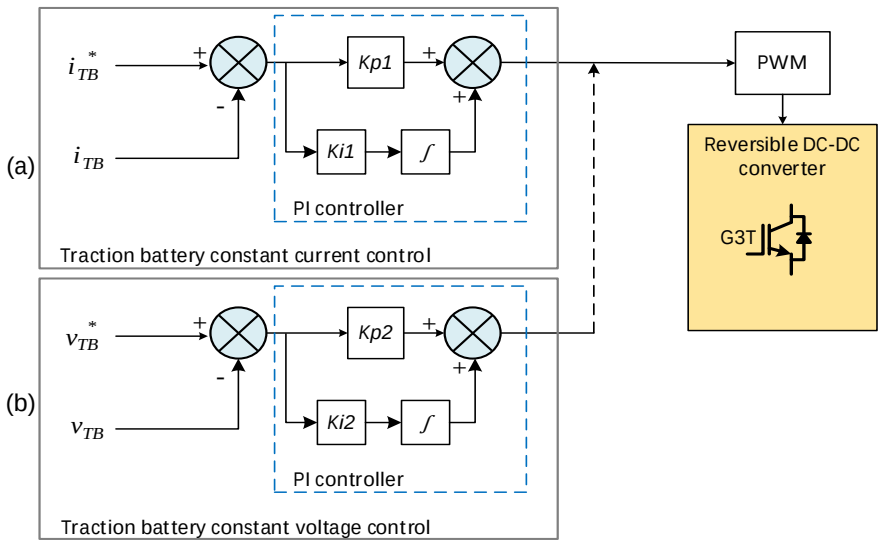


**Figure 8**: Digital controller of the reversible DC-DC converter in the constant current charging mode (a) and constant voltage charging mode (b).

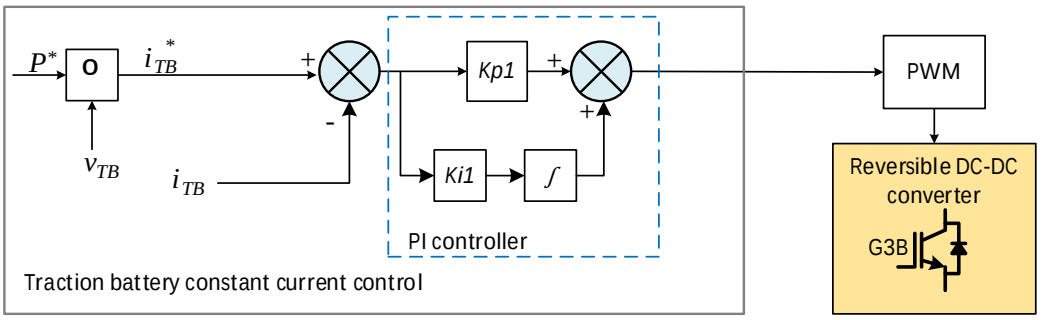


**Figure 9**: The control block diagram of the reversible DC-DC converter digital controller during the V2G operation mode

With the knowledge that the voltage of traction batteries does not significantly change during short-run periods, the constant current supplied by the traction batteries can be used to regulate the active power, which is delivered back to the power grid. Due to a slight decrease caused in the traction batteries' voltage during the discharging procedure, the active power must be maintained constant by proportionate inversely increasing the reference current for the traction batteries. Thus, the reference power ($P^*$ - set up as an external input parameter during the V2G state) should be divided by the voltage ($v_{VB}$) of traction batteries aimed at calculating the reference current ($i_{TB}*$) of traction batteries. The reference is compared with the real current to obtain the traction batteries current; a PI controller is then fed by the resulting error to adjust the output duty-cycle by a PWM modulator equipped with a 40 kHz triangular carrier (Figure 9).

# 4 Result and Discussion

The proposed scheme in this paper is in two parts. The first part is the results of the grid according to the parameter setting of Table 1 without virtual resistor injection. Part two is the case in which a virtual resistor is injected into the grid to improve charge controlling.

## 4.1 Result of Grid without Virtual Resistor Injection.

The proposed scheme in this paper is in two parts. The first part is the results of the grid according to the parameter setting of Table 1 without virtual resistor integration. Part two is that case with a virtual resistor to improve charge controlling. The proposed control strategies set out in the previous sections for different modes of operation of EVs are simulated in MATLAB 2019a and the results are described in this section.

**Table 1**: Selected parameters used in the simulation.

| Parameter | Amount | Parameter | Amount |
|---|---|---|---|
| Capacitor C1 | 5mF | Charger Power | 3 kW |
| inductor L1 | 2mH | Battery Voltage | 300 V |
| inductor L2 | 10mH | Resistor R | 0.2Ω |
| Capacitor C2 | 1mF | Trans Transform ratio | 400:300 |
| PI Controller constants | | | |
| $K_p$ | 2.5 | $K_I$ | 0.005 s |

### 4.1.1 G2V Result

In the G2V performance mode, the charger received power from the network. The reference current for the 10A battery charger is considered. It should be noted that the reactive power value is considered zero. The initial battery charge is considered to be 50% [21].

The voltage changes, the battery current, and the State of Charge (SoC) is the level of charge of an electric battery relative to its capacity.) of the battery in the network mode are shown in Figure 10. As you can see, flow changes are less than 5%.

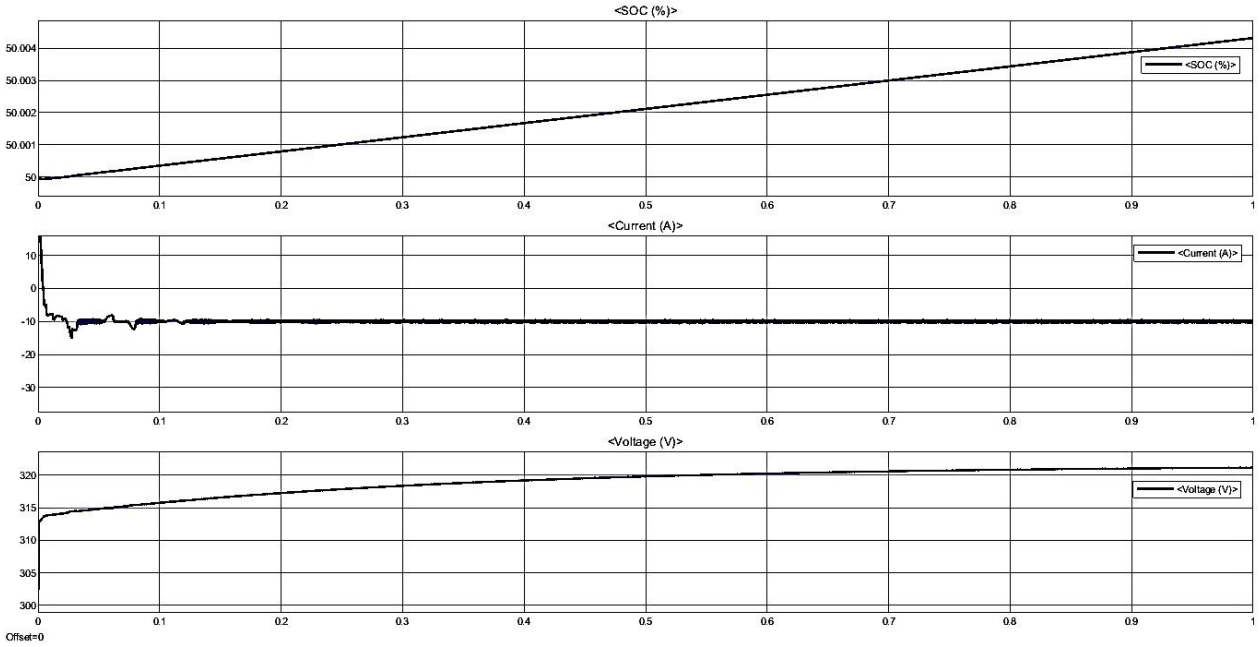


**Figure 10**: SOC, current, and voltage changes of battery in G2V mode.

In Figure 11, the current and voltage input AC and output DC are shown. The phase-to-phase voltage and current indicate the power gain with the unit's power factor of the network. Also as shown in Figure 12, the THD of output current is less than 5%, which is in accordance with the standard which limits THD up to a maximum of 5%.

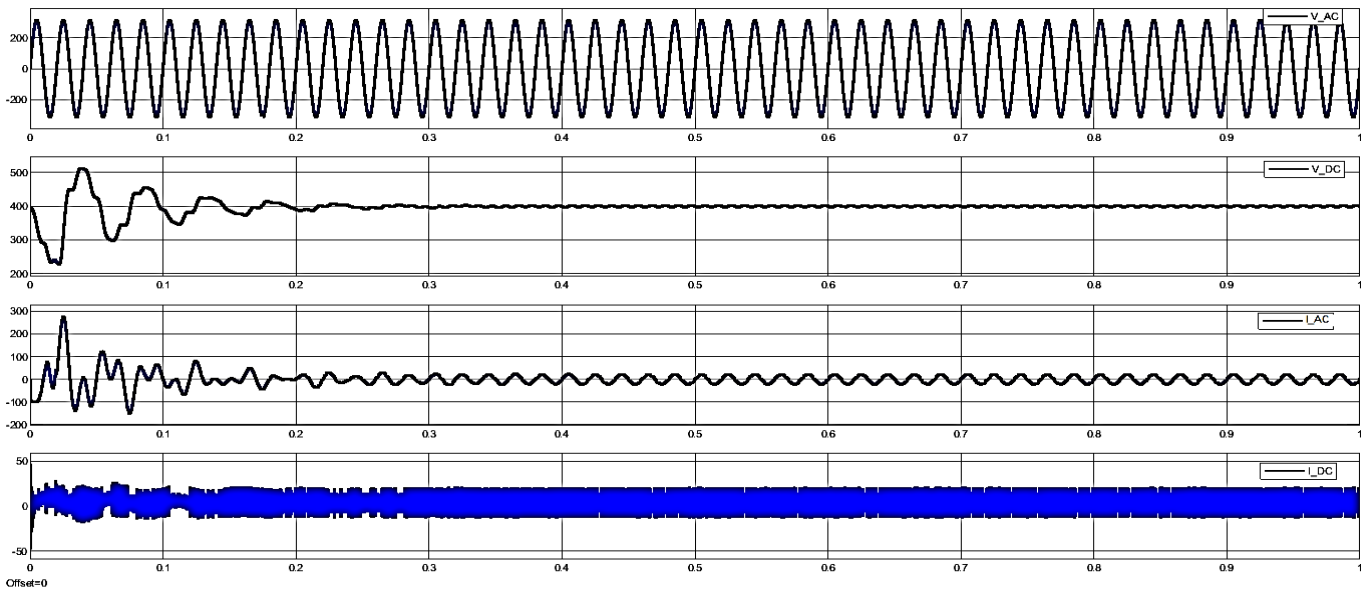


**Figure 11**: View of the voltage and current of the grid input and output in V2G mode.

### 4.1.2 V2G Result

In V2G mode performance, the charger provides power to the network. The full-bridge ac-dc invertor is similar to the G2V mode and the controller for the dc-dc inverter in V2G mode. The reference active power is considered in the V2G is 1 KW. It should be noted that the amount of reactive power in the simulation is considered zero. As shown in Figure 13, the battery charge level is reduced.

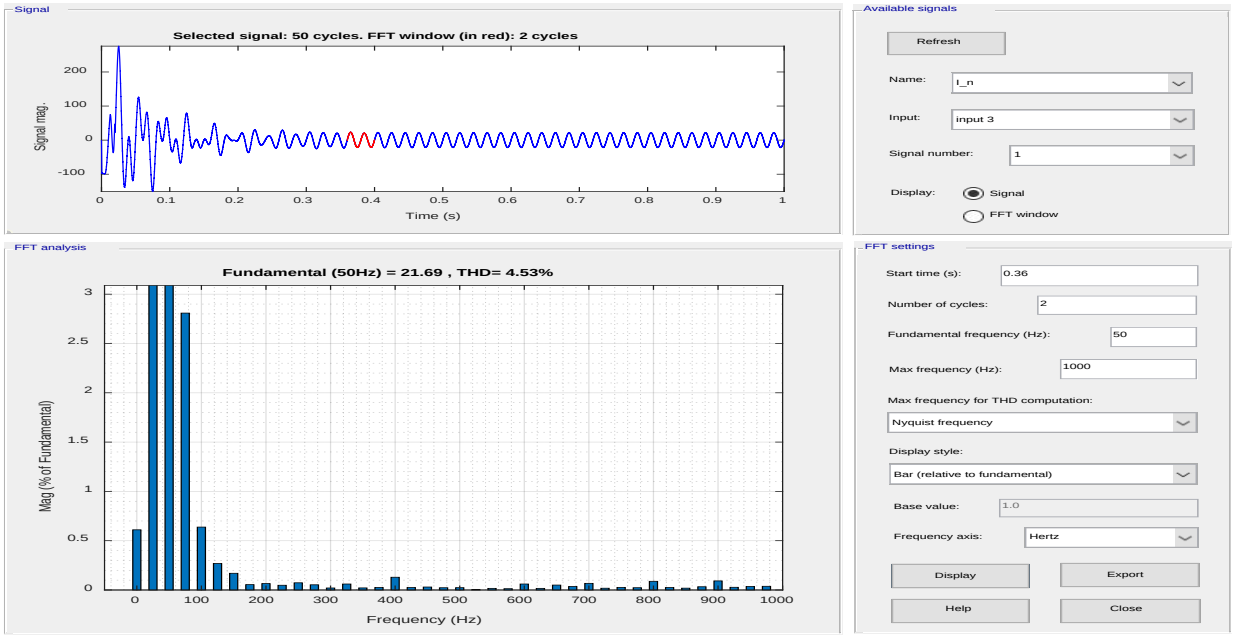


**Figure 12**: Input current of THD in G2V mode.

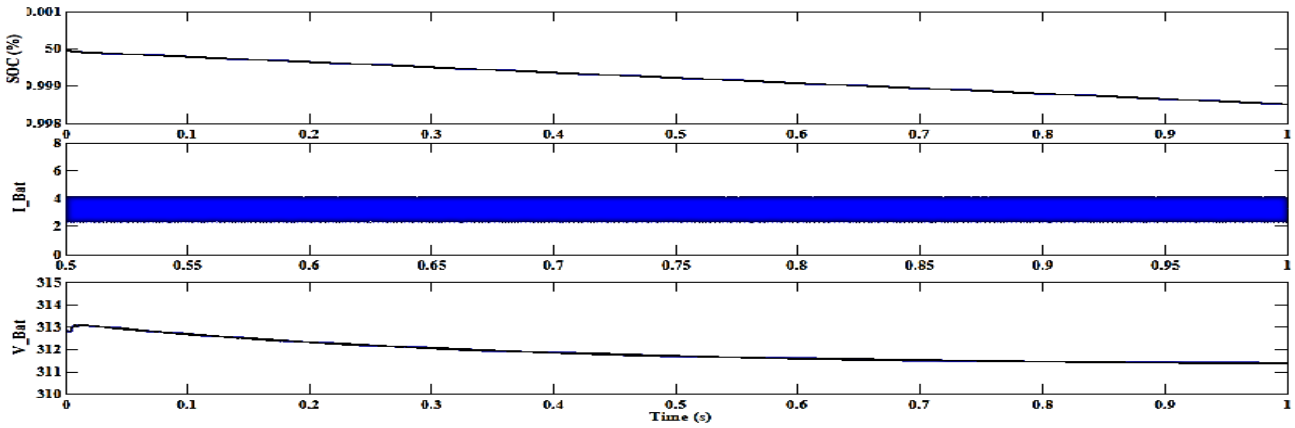


**Figure 13**: Input Voltage and Current and Output Voltage in V2G Mode.

## 4.2 Result of Grid with Virtual Resistor Injection.

We now compare the outputs obtained by simulating the system with the simulation of the system using virtual resistance control. All of the initial parameters and conditions in this simulation are fixed and unchanged. The main purpose of this simulation is to observe the control of the harmonics and noise generated in each of the shown outputs.

The AC/DC controller by using the virtual resistor control system is shown in Figure 14. Now we can run the simulation and provide the result of G2V mode and V2G mode by virtual resistor injection.

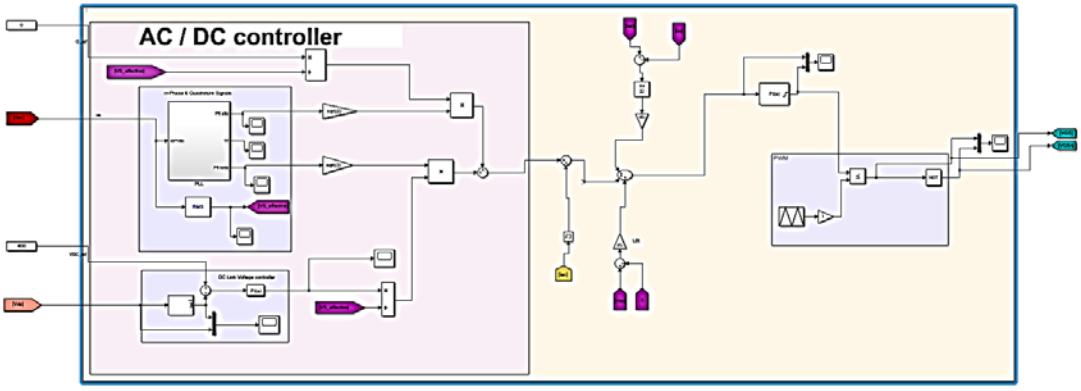


**Figure 14**: AC/DC controller by using of virtual resistor control system

### 4.2.1 G2V Mode Results.

In Figure 15 the voltage changes, the battery current, and the SOC charge status of the battery in this model have shown. By comparing the two modes of this simulation (with and without virtual resistor injection), both of which represent an outline of SOC changes, the current and voltage of the battery in the mode of operation of the G2V, we can conclude that the system examined and considered in the desired. The mode of using virtual resistance control has fewer harmonics in its initial output than the first mode. In Figure 16, the current and voltage of the ac input and dc output have shown.

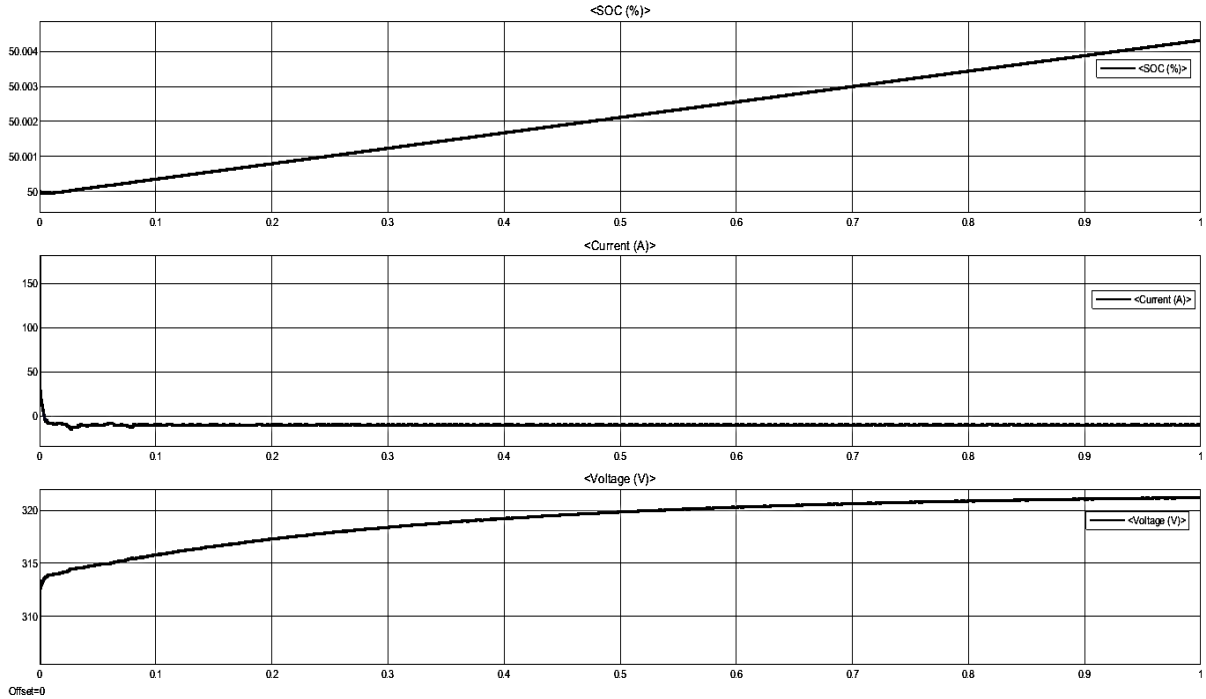


**Figure 15**: View of SOC changes, current, and battery voltage results in G2V mode.

Also, the percentage of THD obtained from the input current of this output is examined in order to observe the reduction of the harmonics in Figure 17. Comparing Figure 17 with Figure 13, the THD of current is 3.66%, which is in accordance with the standard, and this value is 0.86% less than the harmonic value of the system in the first state (without a virtual resistor), so in indicating the suitability of the proposed virtual resistor in this system.

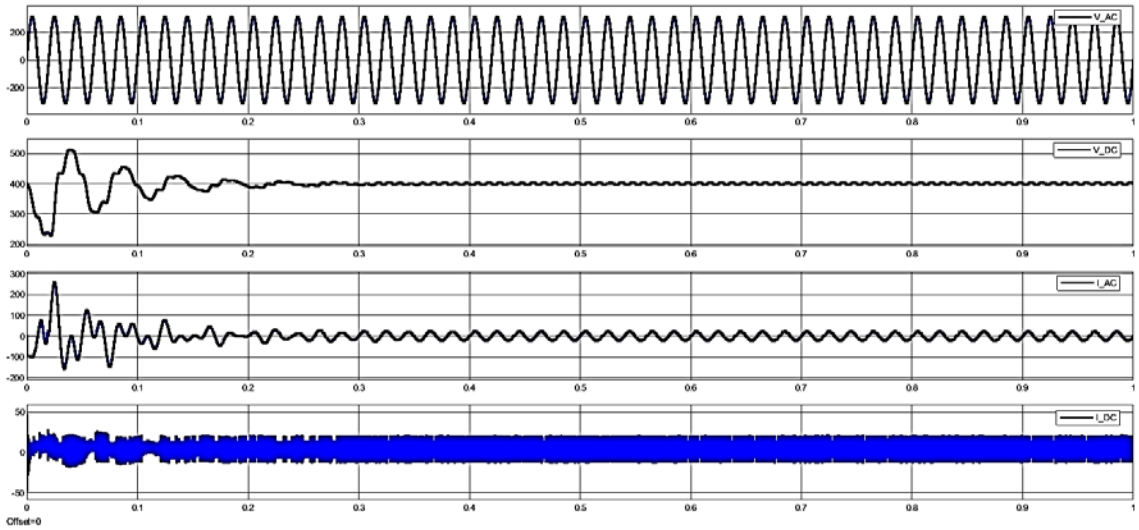


**Figure 16**: AC input voltage and current, and DC voltage and current in G2V mode.

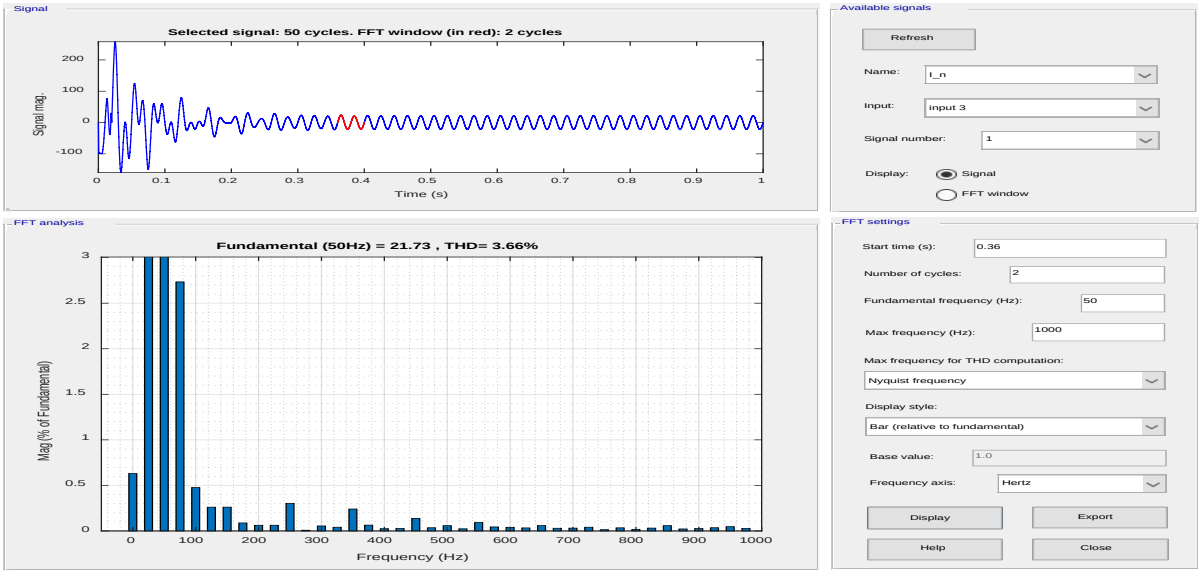


**Figure 17**: THD of the input current in G2V mode.

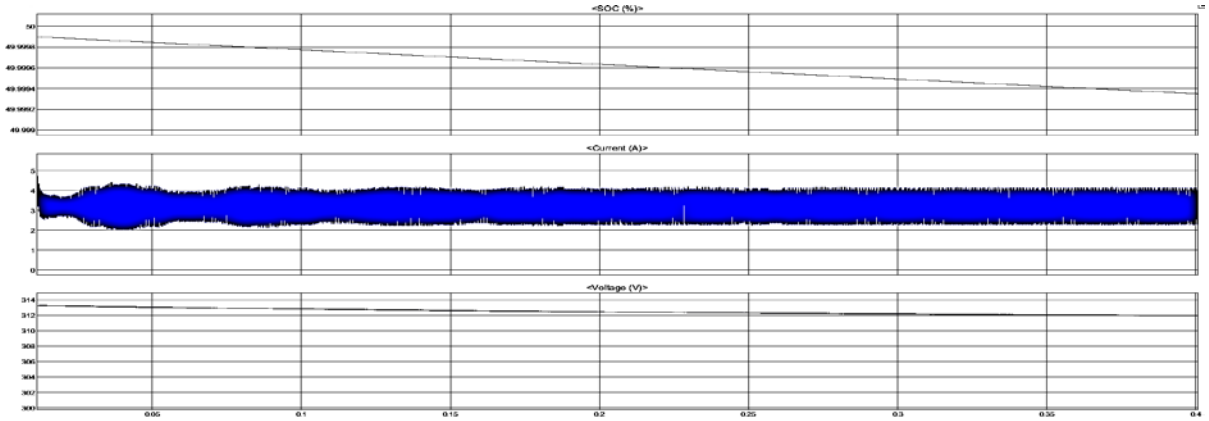


**Figure 18**: Input and output of voltage and current in V2G mode.

### 4.2.2 V2G Mode Results

In this case, the parameters are constant as well as the initial state. In Figure 18 the result of input and output of voltage and current have been shown. As we can see, in this case, the harmonics in the output current are also reduced and the performance of this simulation is more

accurately demonstrated with the help of virtual resistance control. As shown in the results obtained from this simulation, the system has reached stability in the controller area, after applying the virtual resistor, and can control the system in an emergency.

## 5 Conclusion

In this article, an adjustable battery charger is presented for electric vehicles (EVs) with virtual resistor injection, allowing interaction with the grid to charge the G2V batteries followed by the transfer of a portion of their stored energy to the power grid (V2G). The reactive power can be adjusted in both states, which constantly operates with a Sinusoidal waveform current in the whole working spectrum (ranging from the minimum to fully-loaded state), which thereby regulates the voltage of the mains and controls the distortion. A virtual resistor injection control has been controlled to operate with the sinusoidal current. Based on the findings, the charge controller can be improved by connecting the virtual resistor serially or setting a parallel connection between the inductor or capacitor and the virtual resistor. Otherwise stated, findings demonstrate the effectiveness of the introduced technique.

## 6 Availability of Data and Material

Data can be made available by contacting the corresponding author.

## 7 References


[1] S. Haghbin, S. Lundmark, M. Alakula, and O. Carlson, "Grid-connected integrated battery chargers in vehicle applications: Review and new solution," IEEE Transactions on Industrial Electronics, 60(2), pp.459-473, 2013.

[2] M. Yilmaz and P. T. Krein, "Review of battery charger topologies, charging power levels, and infrastructure for plug-in electric and hybrid vehicles," IEEE Transactions on Power Electronics, 28(5), pp.2151-2169, 2013.

[3] A. Khaligh and S. Dusmez, "Comprehensive topological analysis of conductive and inductive charging solutions for plug-in electric vehicles," IEEE Transactions on Vehicular Technology, 61(8), pp.3475- 3489, 2012.

[4] S.-G. Jeong, W.-J. Cha, S.-H. Lee, J.-M. Kwon, and B.-H. Kwon, "Electrolytic Capacitor-Less Single-Power-Conversion On-Board Charger With High Efficiency," IEEE Transactions on Industrial Electronics, 63(12), 7488-7497, 2016.

[5] B. Whitaker, A. Barkley, Z. Cole, B. Passmore, D. Martin, T. R. McNutt, A. B. Lostetter, J. S. Lee, and K. Shiozaki, "A high-density, high efficiency, isolated onboard vehicle battery charger utilizing silicon carbide power devices," IEEE Transactions on Power Electronics, 29(5), 2606-2617, 2014.

[6] D. S. Gautam, F. Musavi, M. Edington, W. Eberle, and W. G. Dunford, "An automotive onboard 3.3-kW battery charger for PHEV application," IEEE Transactions on Vehicular Technology, 61(8), pp.3466-3474, 2012.

[7] S. Kim and F.-S. Kang, "Multifunctional onboard battery charger for plug-in electric vehicles," IEEE Transactions on Industrial Electronics, 62(6), pp. 3460-3472, 2015.

[8] K. Yao, Y. Wang, J. Guo, and K. Chen, "Critical Conduction Mode Boost PFC Converter with Fixed Switching Frequency Control," IEEE Transactions on Power Electronics, 2017.

[10] W. Choi, "Single-stage battery charger without full-bridge diode rectifier for light electric vehicles," Electronics Letters, 47(10), pp. 617-618, 2011.

[11] W.-Y. Choi and J.-S. Yoo, "A bridgeless single-stage half-bridge AC/DC converter," IEEE Transactions on Power Electronics, 26(12), pp.3884-3895, 2011.

[12] Deepak S. Gautam, Fariborz Musavi, Murray Edington, Wilson Eberle, William G. Dunford, "An Automotive Onboard 3.3-kW Battery Charger for PHEV Application," IEEE Trans. Veh. Technol., 61(8), pp.3466-3474, Oct. 2012.

[13] IEEE Trial-Use Standard Definitions for the Measurement of Electric Power Quantities Under Sinusoidal, Nonsinusoidal, Balanced, or Unbalanced Conditions, IEEE Std 1459-2000, Jan. 2000.

[14] Young-Joo Lee, Alireza Khaligh, Ali Emadi, "Advanced Integrated Bidirectional AC/DC and DC/DC Converter for Plug-In Hybrid Electric Vehicles," IEEE Trans. Veh. Technol., 58(8), pp.3970-3970, Oct. 2009.

[15] Sung Young Kim, Hong-Seok Song, Kwanghee Nam, "Idling Port Isolation Control of Three-Port Bidirectional Converter for EVs," IEEE Trans. Power Electron., 27(5), pp.2495-2506, 2012.

[16] Qian T, Shao C, Li X, Wang X, Shahidehpour M. Enhanced Coordinated Operations of Electric Power and Transportation Networks via EV Charging Services. IEEE Transactions on Smart Grid, 11(4): 3019-30, 2020

[17] Bernal R, Olivares D, Negrete M, Lorca Á. Management of EV charging stations under advance reservations schemes in electricity markets. Sustainable Energy, Grids and Networks. 2020 Sep 24:100388.

[18] Ghotge R, Snow Y, Farahani S, Lukszo Z, van Wijk A. Optimized scheduling of EV charging in solar parking lots for local peak reduction under EV demand uncertainty. Energies. 2020 Jan;13(5):1275.

[19] Khalkhali H, Hosseinian SH. Multi-class EV charging and performance-based regulation service in a residential smart parking lot. Sustainable Energy, Grids and Networks. 2020 Apr 20:100354.

[20] Ruddell S, Madawala UK, Thrimawithana DJ. A Wireless EV Charging Topology With Integrated Energy Storage. IEEE Transactions on Power Electronics. 2020 Jan 23;35(9):8965-72.

[21] Pinto JG, Monteiro V, Gonçalves H, Afonso JL. Onboard reconfigurable battery charger for electric vehicles with traction-to-auxiliary mode. IEEE Transactions on vehicular technology. 2013 Sep 25;63(3):1104-16.

[22] Y. Sat and T. Kataoka, State Feedback Control of Current-Type PWMAC to DC Converters, IEEE Trans. Ind. Appl., 29(6), 1993.

**Dr. Ali S. Alghamdi** is an Assistant Professor in the Department of Electrical Engineering, the College of Engineering, Majmaah University, Saudi Arabia. He received his dual B.S. degree (with high honors) in Computer and Electrical Engineering from Lawrence Technological University, Southfield, Michigan, USA, respectively, and an MSc in Electrical and Computer Engineering from Lawrence Technological University, Southfield, Michigan, USA. He received a Ph.D. in Electrical and Computer Engineering from Oakland University, Rochester, Michigan, USA. His research interests include Statistical Digital Signal Processing, Communication Systems, Adaptive Filter, Modern Control in Power System, Optoelectronics Nano-materials in Renewable Energy, and Wireless Sensor Network .Innovation.